ACS OMEGA

http://pubs.acs.org/journal/acsodf

Article

Fractal Analysis of the Distribution and Morphology of Pores in Dinosaur Eggshells Collected in Mexico: Implications to Understand the Biomineralization of Calcium Carbonate

Nerith R. Elejalde-Cadena and Abel Moreno*

Cite This: *ACS Omega* 2021, 6, 7887−7895

Read Online

ACCESS | Metrics & More | Article Recommendations | Supporting Information

ABSTRACT: In this work, we present an investigation of the surface area and roughness of different dinosaur eggshells of 70 million years old using fractal dimension analysis obtained from atomic force microscopy (AFM) and scanning electron microscopy (SEM) information. We also conduct qualitative analyses on the external and inner surfaces of eggshells, which are mainly composed of calcium carbonate. The morphological characteristics of both surfaces can be revealed by both SEM and AFM techniques. It is observed that the inner surface of the eggshell has greater roughness that increases the surface area due to the vaster number of pores compared to the external face, making, therefore, the fractal dimension also greater. The aim of this contribution is to identify the morphology of the pores, as well as the external and inner surfaces of the eggshells, since the morphology is very similar on both surfaces and will otherwise be difficult to determine with the naked eye by SEM and AFM. In addition, the sole AFM analysis is very complicated for these types of samples due to the intrinsic roughness. However, it needs additional methods or strategies to complete this purpose. This contribution used the fractal dimension to show the same behavior obtained in both SEM and AFM techniques, indicating the fractal nature of the structures.

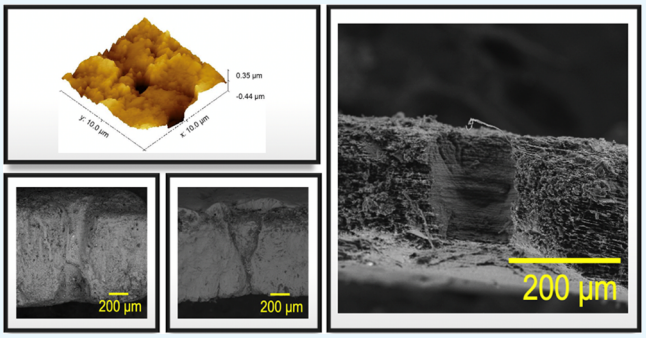

1. INTRODUCTION

An egg is a mineralized structure that fulfills the function of protecting the embryo for its correct growth and development. It is divided into an organic phase (composed mainly of biomacromolecules as proteins) and an inorganic phase (composed mainly of calcium carbonate), and depending on the content of these phases, some eggs can be flexible (turtle eggs), semi-rigid (crocodile eggs) and rigid (chicken eggs). Among the species that are characterized by presenting rigid eggs, we find dinosaurs. Not only dinosaurs' eggs are known to be very rigid, but they are also known to be very thick. Like the other species, they have an inorganic phase called eggshell, developed through the formation of crystalline calcium carbonate ($CaCO_3$) units on the inner eggshell membrane (mammillary cone), initiating the formation of a very rigid structure called mineral palisade, giving way to the formation of pores, which fulfill the function of providing the embryo with a homeostatic medium.[1]

The morphology exhibited by the crystalline units and the pores in the dinosaur eggshells allow us to discern between a variety of eggshells that belong to different species of dinosaurs. Regardless of the species and the type of eggshell, they fulfill the same functions: (1) protection and isolation of the embryo from the external environment, (2) gas exchange produced by respiration and metabolism of the embryo (input of oxygen (O_2)), (3) exchange of water vapor, and (4) thermal exchange from inside to outside and vice versa.[2,3]

According to Russu,[4] the porosity of an eggshell depends on four factors: (1) the number of pores; (2) cross-sectional area; (3) length; (4) pore morphology; and in turn, its direct relation to the fractal dimension.[5] In the eggshell of various species, pores between 0.01 and 1 mm have been observed, which, according to the IUPAC, are classified as macropores (>50 nm). As the pores are smaller and the number of pores contained in the eggshell increases, the specific superficial area of the system (area/volume ratio) also increases dramatically, and so does the roughness.

Fractals have been accepted to describe different natural systems and currently finding extensive application in diverse areas such as telecommunication technology,[6] computer science,[7] optical and electronic devices,[8,9] and recent characterization of absorption capacity, porosity, and surface area,[10,11] using atomic force microscopy (AFM),[12] scanning electron

Received: January 26, 2021
Accepted: March 3, 2021
Published: March 12, 2021

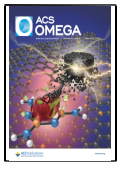

ACS Publications

© 2021 The Authors. Published by American Chemical Society

microscopy (SEM),[11,13] chorioallantonic,[14] extra-embryonic vessels,[15] vascular networks,[16] magnetic resonance images,[17] among others. For example, random systems at the microscopic scale behave like fractals, i.e., their geometrical units resemble one another at all scales (at both low and high magnifications, similar features are identified). It, therefore, means that fractals are not sensitive to the scale of resolution and fractal analysis can be used to extract more information about a surface as compared to the conventional statistical methods. They argued that the presence of low-density regions (a network of pores) of surfaces with microstructures was the reason for the fractal behavior of thin surfaces. In rough surfaces, the fractal dimension is used as an analytical index to measure how the morphological features vary on scaling.[18,19] The fractal analysis provides information on the roughness exponent, correlation length, and shift (or lattice size) These parameters offer a detailed description of spatial patterning, segmentation, texture, and lateral roughness of the surface morphology.[20,21]

On the other hand, it is evident that the porous structures do not have an ordered arrangement in their structure, so it is not trivial to find one. For this, different methods have been developed for the fractal analysis of various systems. According to Mandelbrot:[22] "Fractals can be intuitively defined as objects within objects or the repetition of the same objects at different scales". There are two types of fractals: self-similarity and self-affinity. Self-similarity involves geometric objects whose shape does not change when magnifying at different scales; this means that these objects present regular fractals. Instant self-affinity tends to exist in various natural objects (though not always) that exhibit self-similarity only up to a certain level of magnification or only in certain portions of it,[23,24] e.g., eggshells (Figure 1). The eggshell surface can be seen as a fractal object due to its roughness at different scales.

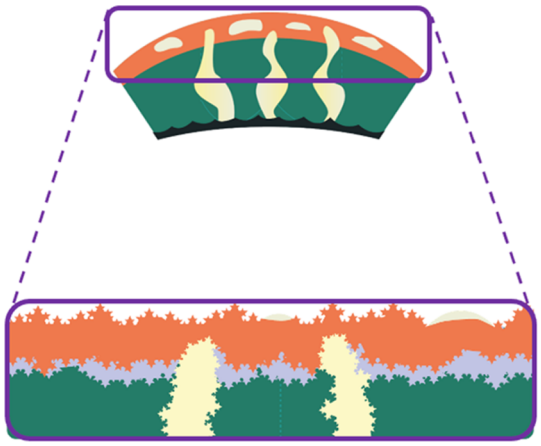

Figure 1. Representation of a typical eggshell surface with fractal behavior (Koch curve). The inset shows a zoom over the surface of the eggshells where the self-affinity is observed.

Of the different methods used to determine the fractal dimension, the most common is the box counting method, which uses a count of the minimum number of boxes N (of size h) necessary to fully cover a graph or figure (in two-dimensional (2D) (SEM) or three-dimensional (3D) (AFM)). The counting process is repeated for different values of h and $\log(N)$ is plotted as a function of $\log(1/h)$. The points obtained are approximated by the traditional method of least squares to a straight line. By the definition of box counting, the fractal dimension is the limit of the ratio $\log(N)/\log(1/h)$ when h tends to zero. This value can be approximated to the magnitude of the slope of the line. Then, for each case, the number of boxes (N) covering the fractal features is counted, and this logarithm is plotted versus the size of boxes (h).[24,25] The fractal dimension (D) is determined from the maximal slope coefficient of the double log plot defined as follow

$$D = \lim_{h \to 0} -\frac{\log N(h)}{\log\ h} \tag{1}$$

Due to the lack of information in the determination of the surface area and roughness of the samples of dinosaur eggshells using the box counting method, the eggshells of different species of dinosaurs that lived in the Late Cretaceous were studied to obtain the analysis of the fractal dimension in 2D and 3D using images obtained by scanning electron microscopy (SEM) and atomic force microscopy (AFM), respectively.

The aim of this contribution is to use the fractal dimension to show the same behavior obtained in both SEM and AFM techniques, indicating the fractal nature of the structures. This contribution will open the possibility of applying this methodology using other images as in the case of optical images for ancient samples, where growth patterns can be mathematically and structurally analyzed.

2. MATERIALS AND METHODS

These ancient eggshells of Late Cretaceous dinosaurs were collected in the coastal area of El Rosario, Baja California in Mexico.[26] These eggshells of different species of dinosaurs were first washed with 5% ethylenediaminetetraacetic acid (EDTA) with the aim of eliminating the organic membrane and then they were washed with Milli-Q water and air-dried. All samples were observed with an SZH10 OLYMPUS microscope on both sides to determine the corresponding sides of the eggshells. The thickness was sized using ImageJ software. For the SEM images, the samples were washed with 5% EDTA and Milli-Q water and then air-dried. We used a TESCAN VEGA 3 SB microscope with a voltage range of 10−20 kV at high vacuum at magnifications of 500× and 1000×. The SEM images at a magnification of 500× were observed with Digital Micrograph software to observe the size of the pores on both sides of the eggshells, while the images at a magnification of 1000× were converted into binary images using ImageJ software. The SEM images of the cross section were taken after the treatment of the samples using a sandpaper of 1500 grit with the aim of observing the pores. After that, the fractal dimension of binary images was determined using the box counting method. Then, a NanoScope V from Thermo was used for AFM. The images in three-dimensional color graphics were obtained using ScanAsyst-air tips in scan assist mode at different scanning rates with NanoScope 9.2 software, and the surface area, mean roughness, and fractal dimension of every sample were processed with Gwyddion software.

3. RESULTS AND DISCUSSION

During the past years, fossils of different dinosaur species have been recorded in Mexico. Among these records is the collection of eggshells in the town of El Rosario, Baja California, corresponding to the Late Cretaceous (74 MY).

https://dx.doi.org/10.1021/acsomega.1c00478
ACS Omega 2021, 6, 7887−7895

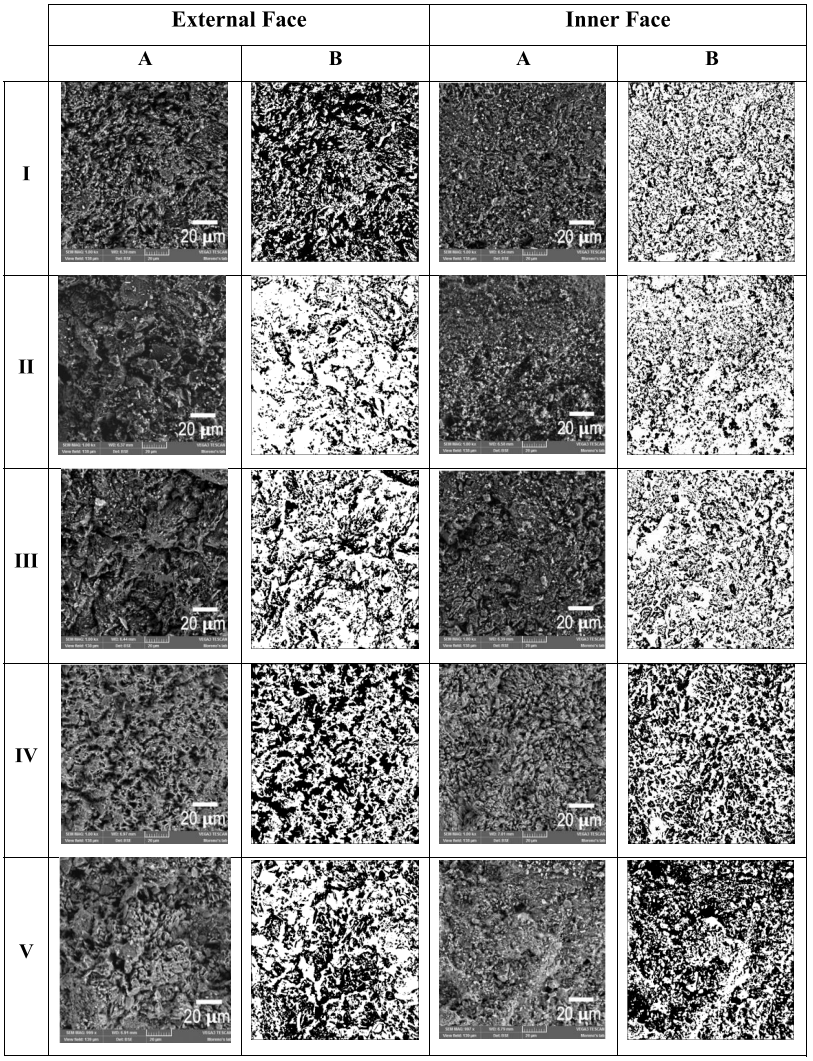

Figure 2. SEM images using box counting analysis. (A) SEM images at 1000× and (B) binary images. (I) *Spheroolithus* sample 1, (II) Lambeosaurinae eggshell, (III) *Spheroolithus* sample 2, (IV) *Prismatoolithus*, and (V) nonidentified ootaxon.

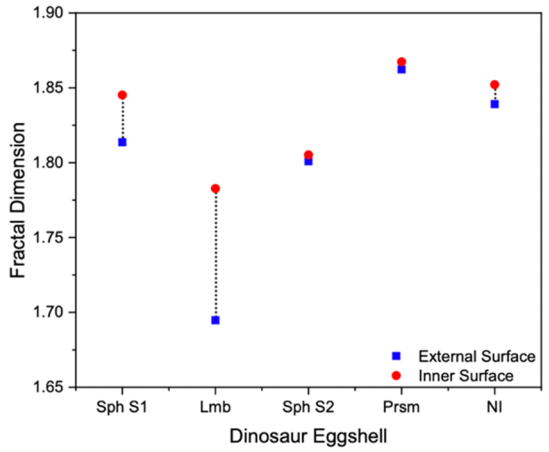

Figure 3. Fractal dimension based on eggshell SEM images. Sph S1: *Spheroolithus* sample 1, Lmb: Lambeosaurinae eggshell, Sph S2: *Spheroolithus* sample 2, Prsm: *Prismatoolithus*, and NI: nonidentified ootaxon. Fractal dimension (D) values are between 1.69 and 1.87.

Some samples of eggshells belong to ornithopod (herbivores) and theropod (carnivores) dinosaurs of the Hadrosauridae and Troodontidae families, respectively. Those of the Hadrosauridae family correspond to the oogenus *Spheroolithus*, and the oogenus *Prismatoolithus* correspond to the Troodontidae family.[26] The prefixes "oo" (egg) and "*oolithus*" (stone egg) are added to differentiate oospecies, oogenus, and oofamilies of dinosaurs.[27,28]

We analyzed two eggshells of the oogenus *Spheroolithus* (samples 1 (I) and 2 (III)); one of the family Lambeosaurinae (II), which is part of the Hadrosauridae family, with the oogenus nonidentified; one of the oogenus *Prismatoolithus* (IV); and one nonidentified ootaxon (V).

SEM images were taken from both sides of the eggshell to observe the homogeneity of the sample, witnessing larger structures on the external surface of the eggshell and superficial roughness, while for the inner surface, the observed structures are smaller, giving a smooth and homogeneous appearance compared to the external surface. In addition, using SEM images at 1000×, binary images were obtained to get information about the shape and size of the pores of the eggshells (dark areas, Figure 2B), which have different morphologies and sizes, being wider than those observed on the external face.

Based on the binary images, the fractal dimension was calculated (Figure 3) using a logarithm based on the

https://dx.doi.org/10.1021/acsomega.1c00478
ACS Omega 2021, 6, 7887−7895

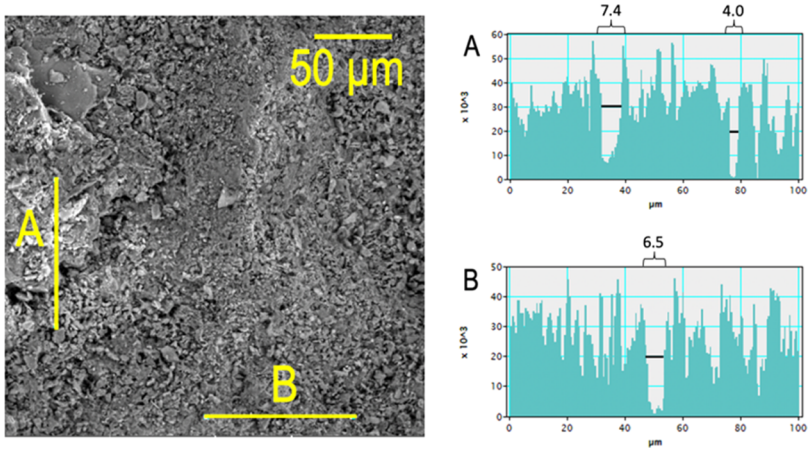

Figure 4. SEM images and roughness profile indicating the possible pores of the external face of the eggshell of the *Spheroolithus* sample 1. (A) Vertical profile and (B) horizontal profile.

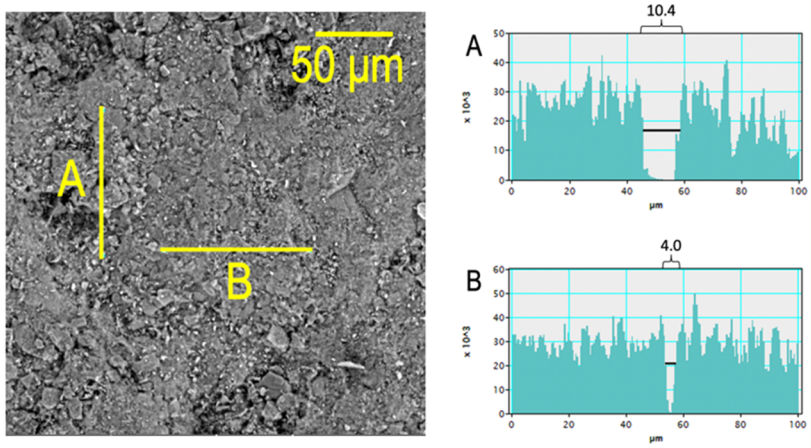

Figure 5. SEM images and roughness profile indicating the possible pores of the internal face of the eggshell of the *Spheroolithus* sample 1. (A) Vertical profile and (B) horizontal profile.

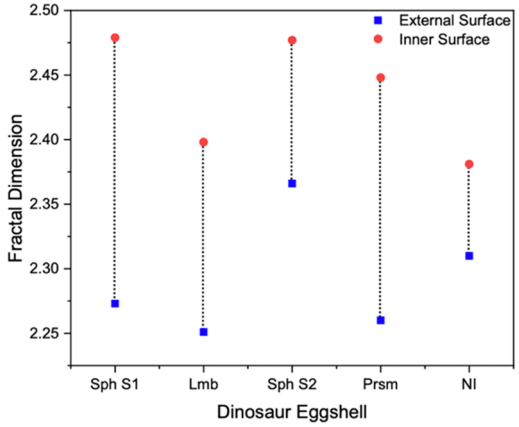

Figure 6. Fractal dimension based on AFM images. Sph S1: *Spheroolithus* sample 1, Lmb: Lambeosaurinae eggshell, Sph S2: *Spheroolithus* sample 2, Prsm: *Prismatoolithus*, and NI: nonidentified ootaxon. Fractal dimension (D) values are between 2.25 and 2.5, indicating high roughness.

relationship between the number of an empty box ($N(h)$) and the size of the box (h) (eq 1). The eggshells of the *Spheroolithus* sample 2 (Sph S2) and *Prismatoolithus* (Prsm) species present a similar pore-size distribution on both surfaces, which could indicate that the pore has a unique entrance and exit, granting greater roughness, but not necessarily a high surface area, just like the one seen in the eggshell of the nonidentified ootaxon (NI). Instead of the other two eggshells, *Spheroolithus* sample 1 (Sph S1) and Lambeosaurinae (Lmb), the difference in roughness observed is greater, compared to the other three samples. This is probably due to wear caused by diagenetic changes during fossilization processes, which allowed the formation of large structures and the fragmentation of the same sample. This causes an increase in the roughness as well as in the hollow areas, interfering with the data, as it is mainly observed in the Lambeosaurinae eggshell (Lmb).

Due to the results obtained by calculating the fractal dimension, it was decided to determine the pore size observed from the SEM images (Figures 4 and 5), which were measured using Digital Micrograph software, where the pores on the inner surface are smaller in diameter than those observed on the external surface. This procedure was performed on all the five dinosaur eggshells (see the Supporting Information) and the same pattern was repeated.

An accurate analysis of the morphology and roughness of the surfaces as well as the calculation of the surface area and many other parameters can be obtained from atomic force microscopy (AFM); this technique is very accurate compared

https://dx.doi.org/10.1021/acsomega.1c00478
ACS Omega 2021, 6, 7887−7895

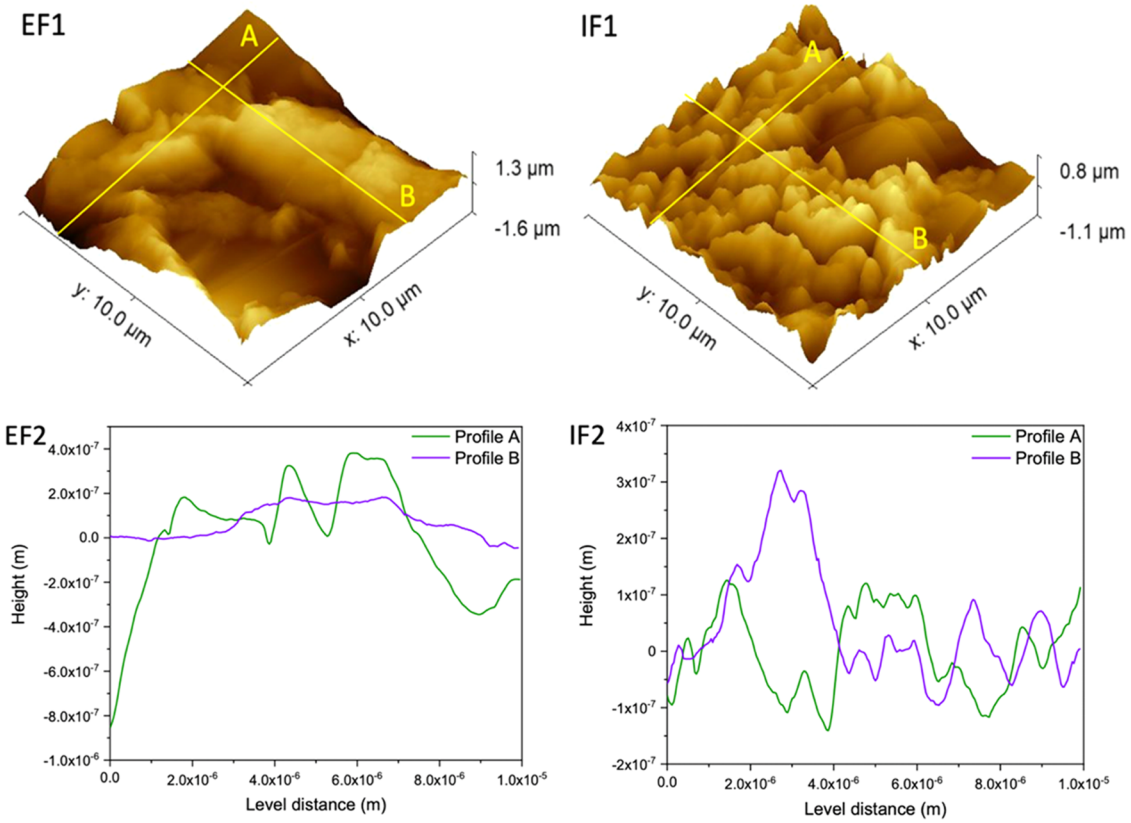

Figure 7. Topographies and profiles of the pore size of the surface of the eggshell of the *Spheroolithus* sample 1. EF: External surface and IF: inner surface. (1) AFM image and (2) profiles of the superficial structure. (A) Profile corresponding to the *X*-axis and (B) Profile corresponding to the *Y*-axis.

to SEM analysis, mainly when samples under analysis are not good conductors. A disadvantage in AFM occurs when the samples under study are very rough, making the interpretation of the results difficult, so other tools must be used for a good interpretation of the results. Such is the case of fractal analysis giving good statistical results to help the characterization of samples like those discussed in this work. The fractal dimension (between 2D and 3D) was determined using AFM images, and the results were similar to those obtained by SEM (fractal dimension between one-dimensional (1D) and 2D), where the inner surface presents a greater roughness. The values obtained between each of the phases are far from each other since with the fractal dimension in AFM, not only the surface but also the volume of the amount of matter present on the surface of the samples, is analyzed up to a few microns deep. According to Figure 6, the *Spheroolithus* eggshells (Sph S1 and S2) show greater roughness (fractal dimension 2D−3D close to 3) in general compared to the other species, followed by Lambeosaurinae (Lmb) and *Prismatoolithus* (Prsm) eggshells, and finally, the nonidentified ootaxon (NI), which presents low roughness on the external surface and decreases on the inner surface.

The roughness data can be confirmed with the profiles obtained from the topographies taken by AFM, where it can be seen that the inner surface presents greater roughness reflected in the variety of size of the observed structures (Figures 7-IF1 and 8-IF1), while the external one presents large structures, giving an almost smooth appearance to the surface (Figures 7-EF2 and 8-EF2), indicating that the formation of structures was a little more ordered and slower, allowing a low variation in the size of the structures present on the surface. This behavior could be observed in the vertical and horizontal profiles (Figures 7 and 8) made on both surfaces of each eggshells (for other species, see the Supporting Information). In addition, for the Lambeosaurinae eggshell (Figure S9-IF1), it was possible to capture the topography of a pore with a diameter of approximately 1.5 μm.

Finally, the roughness was confirmed by calculating the surface area of each eggshell (Figure 9). It is indeed confirmed that the inner surface is rougher, presenting a relationship with the size of the pores determined by SEM images that the larger the pore diameter the less the roughness present on the surface. Therefore, the relationship between the surface area and the fractal dimension is directly proportional (Figure 10).

The results are an indication that the structures and pores present in the inner surface of the eggshells are smaller; however, when they are found in abundance, they increase the roughness. This conclusion was corroborated through the analysis of the distribution of the pores using the binary images obtained from SEM, which were analyzed using ImageJ software, for all of the samples under study (Figure 11). From these images, the range of the pore diameter was determined for the eggshell of the *Spheroolithus* sample 1 (Figure 11, black); it presented in the external surface pores with diameters between 1.1 and 1.3 μm (Figures 11-1A), while on the inner surface, the pore size was smaller with approximately a diameter of 1 μm (Figures 11-1B). Similar results were obtained from the eggshells of Lambeosaurinae (Figure 11, red) and *Spheroolithus* sample 2 (Figure 11, blue),

https://dx.doi.org/10.1021/acsomega.1c00478
ACS Omega 2021, 6, 7887−7895

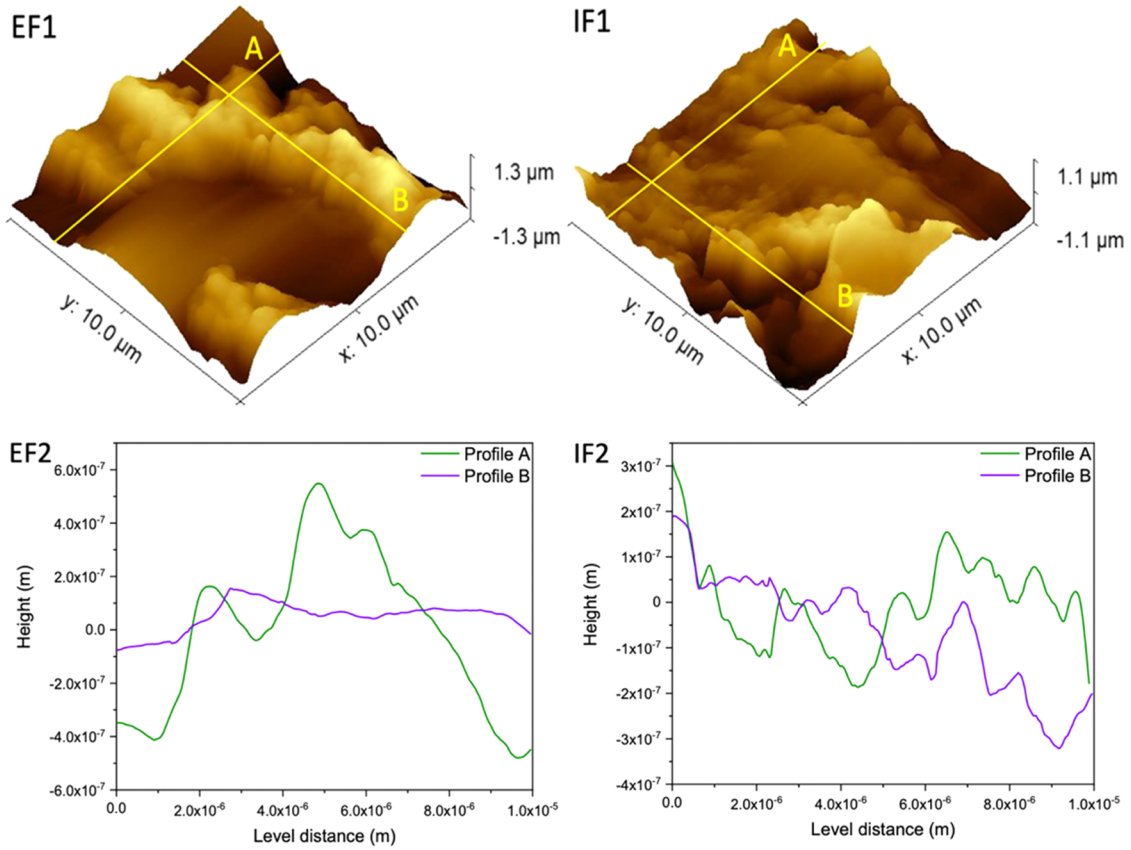

Figure 8. Topographies and profiles of the pore size of the surface of the *Prismatoolithus* eggshell. EF: External surface and IF: inner surface. (1) AFM image and (2) profiles of the superficial structure. (A) Profile corresponding to the *X*-axis and (B) profile corresponding to the *Y*-axis.

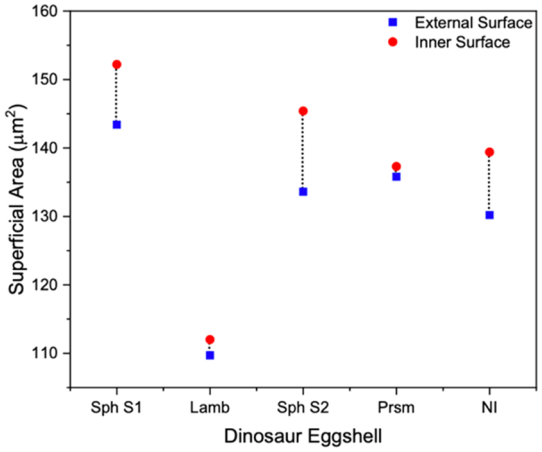

Figure 9. Surface area based on AFM images. Sph S1: *Spheroolithus* sample 1, Lmb: Lambeosaurinae eggshell, SpH S2: *Spheroolithus* sample 2, Prsm: *Prismatoolithus*, and NI: nonidentified ootaxon. For tabulated data, see Table S2.

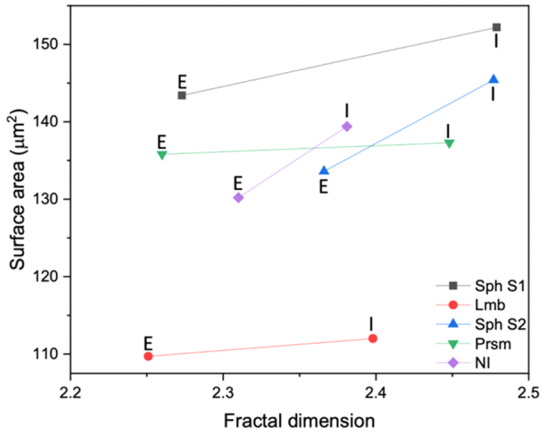

Figure 10. Correlation between the fractal dimension and the surface area of the dinosaur eggshells under study. (E) External surface, (I) inner surface. Sph S1: *Spheroolithus* sample 1, Lmb: Lambeosaurinae eggshell, Sph S2: *Spheroolithus* sample 2, Prsm: *Prismatoolithus*, and NI: nonidentified ootaxon.

with the difference that the latter presented bigger pores on the external surface compared to the other two species.

While *Prismatoolithus* (Figure 11, green) and unidentified ootaxon (Figure 11, purple) presented values of approximately 1−2 and 1.3−1.8 μm for the external surface and 1.8−2.2 and 1.2−1.5 μm for the inner surface, respectively, being the largest in diameter.

These values, compared to those reported by Carpenter (Table 1),[29] are consistent despite the fossilization processes,[30,31] such as recrystallization of calcium carbonates pedogenic[32] or hydrothermal fluids caused mainly by volcanism,[33] which induced the formation of irregular structures, not typical of the eggshell that adhered to the surfaces, causing the deformation of the eggshell microstructures (crystalline aggregates), which hinders the visibility of the pores or the total coverage of them. This same fact increases the roughness value, increasing the surface area of both surfaces of the eggshell with the passing of the years.

https://dx.doi.org/10.1021/acsomega.1c00478
ACS Omega 2021, 6, 7887−7895

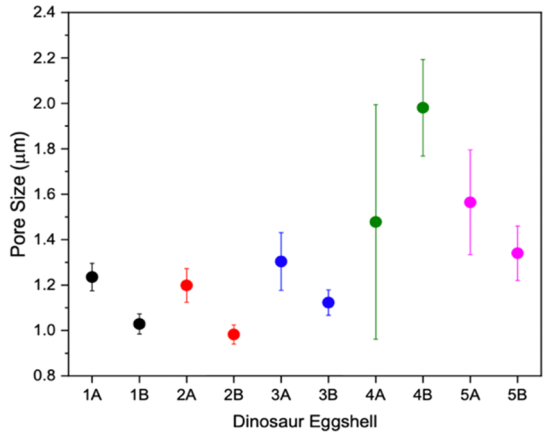

Figure 11. Pore distribution using ImageJ of the eggshell of the dinosaur eggshell under study. (A) External surface and (B) inner surface. (1) *Spheroolithus* sample 1 (black), (2) Lambeosaurinae eggshell (red), (3) *Spheroolithus* sample 2 (blue), (4) *Prismatoolithus* (green), and (5) nonidentified ootaxon (purple).

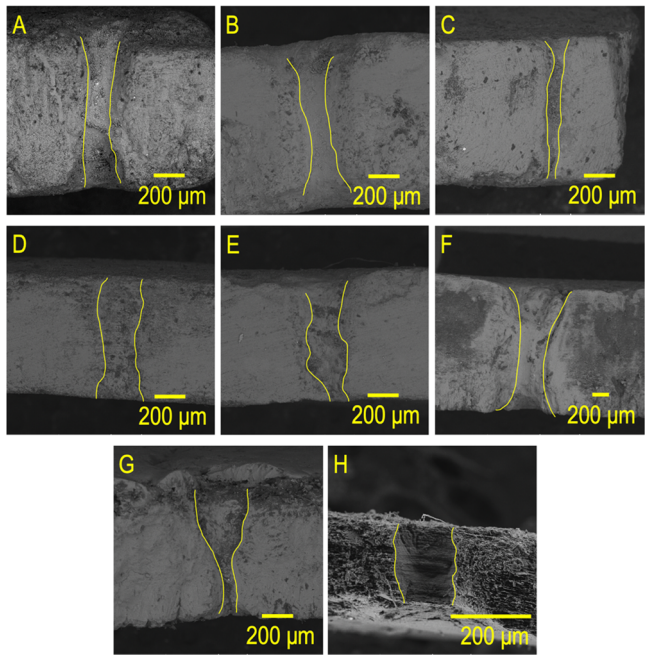

Figure 12. Morphology of the pores of the dinosaur eggshells under study and the phylogenetically related species. (A) *Spheroolithus* sample 1, (B) Lambeosaurinae eggshell, (C) *Spheroolithus* sample 2, (D) *Prismatoolithus*, (E) nonidentified ootaxon, (F) ostrich, (G) emu, and (H) crocodile.

In addition, the morphology of the pores of each of the eggshells under study was observed, which is related to the pore size determined in Figure 6. Figure 12A corresponding to the *Spheroolithus* sample 1 presents a pore with a diameter of approximately 200 μm, with a larger cavity on the external surface of the inner one. The Lambeosaurinae eggshell (Figure 12B), which despite having a slightly narrower diameter, presents a morphology similar to that observed in the *Spheroolithus* sample 1, and following Carpenter's theory, the appropriate pore for these two samples is tubocanaliculate (Figure 13B) with a canal size of 0.5−0.2 mm. In addition, *Spheroolithus* sample 2, which belongs to the same family as the two previous species, presents a difference in the morphology and pore size (Figure 12C). In this case, the pore has a diameter of approximately 100 μm, which corresponds to multicanaliculate (Figure 13C) with a canal size of 0.1−0.3 mm. Both the tubocanaliculate and multicanaliculate pores show a high exchange with the environment due to the conditions in which the eggs were found at the time of deposition, which would be humid environments, with or without sunlight. On the other hand, another type of pore is observed in *Prismatoolithus* and unidentified ootaxon (Figure 12D,E), where the observed pore is prolatocanaliculate (Figure 13D), which is characterized by having a diameter and a variable morphology, as well as the environment in which the eggs were deposited.

Subsequently, the pores of the eggshells of current species such as ostrich, emu, and crocodile (Figure 12) were determined to observe the variability of the pores in other species. Ostrich and emu (Figure 12F,G), species that correspond to the same family, have pores with different morphologies. This result can be taken as evidence to indicate that the morphology of the pores is not related to the species of the same family. At the same time, the ostrich and crocodile eggshells (Figure 12F,H) present a similarity with the *Spheroolithus* sample 1 and Lambeosaurinae eggshells. On the other hand, the pores observed in the emu eggshell have a rimocanaliculate morphology (Figure 13E), which is characterized by having a funnel shape with an external diameter much greater than the internal diameter. This type of pore is suitable for depositions in dry environments.

4. CONCLUSIONS

The correlation of information obtained between the two techniques used (SEM and AFM), using the analysis of the fractal dimension by the box counting method, allowed us to determine the morphology of the structures present on the surface as well as the size of the pores from the binary images (black areas) and the morphology of the pores from the cross-sectional images. In addition, it was identified that the pores on the inner surface of the eggshell have pores of smaller diameters, favoring the formation of smaller structures and therefore giving greater roughness and surface area, evidencing the relationship between the fractal dimension (1D and 2D) and the surface area.

Table 1. Distribution of Every Pore Presents in the Eggshell of Dinosaurs[29]

pore name	canal size (mm)	abundance (mm^2)	exchange	environment
angusticanaliculate	0.01−0.1	3−20/100	less	dried
tubocanaliculate	0.5−0.2	400−500/100	high	buried in humid mounds
multicanaliculate	0.1−0.3	600−1000/100	high	humid mounds
prolatocanaliculate	0.05−1	30−150/100	moderate	varied
rimocanaliculate	0.01−0.03	undefined	undefined	dried
obliquicanaliculate	undefined	undefined	undefined	undefined

https://dx.doi.org/10.1021/acsomega.1c00478
ACS Omega 2021, 6, 7887−7895

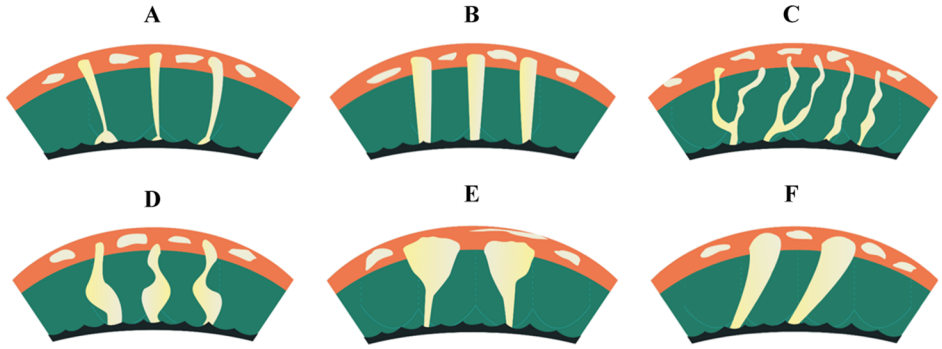

Figure 13. Design of the pores present in dinosaur eggshells. (A) Angusticanaliculate, (B) tubocanaliculate, (C) multicanaliculate, (D) prolatocanaliculate, (E) rimocanaliculate, and (F) obliquicanaliculate.[29]

These analyzes were developed with the purpose of obtaining information about the distribution of the pores and roughness of the eggshells of dinosaurs, contributing to research focused on the analysis of surfaces that present a certain degree of roughness and fractality in different materials. Furthermore, identifying the external and inner surfaces of fossilized eggshells, using methods that are available to everyone, could be a great contribution to the paleontology area, mainly because this methodology could be applied to images that are easier to acquire, such as optics.

■ ASSOCIATED CONTENT

Supporting Information

The Supporting Information is available free of charge at https://pubs.acs.org/doi/10.1021/acsomega.1c00478.

SEM and AFM images to determine the roughness and fractal dimension on both surfaces of the eggshells; determination of porosity and pore size by scattering electron microscopy (SEM) and atomic force microscope (AFM) (S.1); fractal dimension of both surfaces of the eggshells of dinosaurs using SEM binary images and AFM images (Table S1); SEM images and roughness profile indicating the pore of the external surface of the Lambeosaurinae eggshell. (A) Vertical profile and (B) horizontal profile (Figure S1); SEM images and roughness profile indicating the pore of the inner surface of the Lambeosaurinae eggshell. (A) Vertical profile and (B) horizontal profile (Figure S2); SEM images and roughness profile indicating the pore of the external surface of the eggshell of the *Spheroolithus* sample 2. (A) Vertical profile and (B) horizontal profile (Figure S3); SEM images and roughness profile indicating the pore of the inner surface of the eggshell of the *Spheroolithus* sample 2. (A) Vertical profile and (B) horizontal profile (Figure S4); SEM images and roughness profile indicating the pore of the external surface of the *Prismatoolithus* eggshell. (A) Vertical profile and (B) horizontal profile (Figure S5); SEM images and roughness profile indicating the pore of the inner surface of the *Prismatoolithus* eggshell. (A) Vertical profile and (B) horizontal profile (Figure S6); SEM images and roughness profile indicating the pore of the external surface of the eggshell of the nonidentified ootaxon. (A) Vertical profile and (B) horizontal profile (Figure S7); SEM images and roughness profile indicating the pore of the inner surface of the eggshell of the nonidentified ootaxon. (A) Vertical profile and (B) horizontal profile (Figure S8); topographies and profiles of the pore size of the surface of the Lambeosaurinae eggshell. (EF) External surface and (IF) inner surface. (1) AFM image and (2) profiles of the superficial structure. (A) Profile corresponding to the *X*-axis and (B) profile corresponding to the *Y*-axis (Figure S9); topographies and profiles of the pore size of the surface of the eggshell of the *Spheroolithus* sample 2. (EF) External surface and (IF) inner surface. (1) AFM image and (2) profiles of the superficial structure. (A) Profile corresponding to the *X*-axis and (B) profile corresponding to the *Y*-axis (Figure S10); topographies and profiles of the pore size of the surface of the eggshell of the nonidentified ootaxon. (EF) External surface and (IF) inner surface. (1) AFM image and (2) profiles of the superficial structure. (A) Profile corresponding to the *X*-axis and (B) profile corresponding to the *Y*-axis (Figure S11); and superficial area and mean roughness of dinosaur eggshells based on AFM images (PDF)

■ AUTHOR INFORMATION

Corresponding Author

Abel Moreno − *Instituto de Química, Universidad Nacional Autónoma de México, Ciudad de México 04510, México;* orcid.org/0000-0002-5810-078X; Email: carcamo@unam.mx

Author

Nerith R. Elejalde-Cadena − *Instituto de Química, Universidad Nacional Autónoma de México, Ciudad de México 04510, México*

Complete contact information is available at: https://pubs.acs.org/10.1021/acsomega.1c00478

Author Contributions

The manuscript was designed and written through contributions of all authors. All authors have given approval to the final version of the manuscript.

Notes

The authors declare no competing financial interest.

■ ACKNOWLEDGMENTS

One of the authors (N.R.E.-C.) thanks CONACYT (Registration no. 889262) for the scholarship for the Ph.D. program in Chemistry Sciences of Universidad Nacional Autonoma de Mexico and to the Graphic Designer Michelle Dayana Betancourt Pardo for the design of Figures 1 and 13,

https://dx.doi.org/10.1021/acsomega.1c00478
ACS Omega 2021, 6, 7887−7895

corresponding to the types of the pores and representation of the Koch curve. One of the authors (A.M.) acknowledges DGAPA-UNAM project PAPIIT IG200218 for the support of this research. The authors acknowledge Antonia Sánchez-Marín for the English style correction and grammar revision of this contribution.

REFERENCES

(1) Barret, P. M.; Canudo, J. I.; Coria, R. A.; Chiappe, L. M.; Galobart, Á.; Moratalla, J. J.; Pereda, X.; J. de Ricqlès, A.; Royo-Torres, R.; Sanz, J. L.; Weishampel, D. B.; Zhou, Z. *Los dinosaurios en el siglo XX. Nuevas Respuestas al Inagotable Enigma de los Dinosaurios*; Metatemas Tusquets Co Pte Ltd: Barcelona, 2007.

(2) Romanoff, A. L.; Romanoff, A. J. *The Avian Egg*; John Wiley & Sons Co Pte Ltd: New York, 1963.

(3) Board, R. G. Properties of avian eggshells and their adaptative value. *Biol. Rev.* **1982**, *57*, 1−28.

(4) Russu, M. V.; Gheorghiu, S. Fractal-like Features of Dinosaur Eggshells. In *Fractals in Biology and Medicine*,Losa, G. A.; Merlini, D.; Nonnenmacher, T. F.; Weibel, E. R., Eds.; CRC Press: Springer, 2005; pp 245−256.

(5) Peng, C.; Zou, C.; Yang, Y.; Zhang, G.; Wang, W. Fractal analysis of high rank coal from southeast Qinshui basin by using gas adsorption and mercury porosimetry. *J. Pet. Sci. Eng.* **2017**, *156*, 235−249.

(6) Karhana, M.; Kumar, R. A review on fractal antenna. *Int. J. Eng. Res. Technol.* **2017**, *5*, 1−4.

(7) Sala, N. Fractals, Computer Science and Beyond. In *Complexity Science, Living Systems, and Reflexing Interfaces: New Models and Perspectives*,Orsucci, F.; Sala, N., Eds.; CRC Press: Hershey, 2012.

(8) Graydon, O. A light ride to the stars. *Nature* **2019**, *13*, 227−228.

(9) Fan, J. A.; Yeo, W. H.; Su, Y.; Hattori, Y.; Lee, W.; Jung, S. Y.; Zhang, Y.; Liu, Z.; Falgout, L.; Bajema, M.; Coleman, T.; Gregoire, D.; Larsen, R. J.; Huang, Y.; Rogers, J. A.; Cheng, H. Fractal design concepts for stretchable electronics. *Nat. Commun.* **2014**, *5*, No. 3266.

(10) Tao, S.; Pan, Z.; Chen, S.; Tang, S. Coal seam porosity and fracture heterogeneity of marcolithotypes in the Fanzhuang Block souther Qinshui Basin, China. *J. Nat. Gas Sci. Eng.* **2019**, *66*, 148−158.

(11) Zhang, K.; Wang, S. Determination of the box-counting fractal dimension of pore distribution in eggshell based on scanning electron microscopy image analysis. *Adv. Mater. Res.* **2012**, *341−342*, 776−779.

(12) Bramowicz, M.; KŁysz, S. Application of atomic force microscopy (AFM) in the diagnosis of a surface layer. *Res. Works Air Force Inst. Technol.* **2007**, *22*, 167−174.

(13) Smith, T. G., Jr.; Lange, G. D.; Marks, W. B. Fractal methods and results in cellular morphology−dimensions, lacunarity and multifractals. *J. Neurosci. Methods* **1996**, *69*, 123−136.

(14) Chan, Y. K.; Yu-Siw, L.; Meng-Hsiun, T.; Mao-Hsiang, C. Vessel box counting dimension of chicken chorioallantoic images. *Int. J. Comput. Consum. Control* **2016**, *5*, 26−40.

(15) Borba, F. K. S. L.; Loos Queiroz Felix, G.; Ventura Lola Costa, E.; Silva, L.; Dias, P. F.; Albuquerque Nogueira, R. Fractal analysis of extra-embryonic vessels of chick embryos under the effect of glucosamine and chondroitin sulfates. *Microvasc. Res.* **2016**, *105*, 114−118.

(16) Mancardi, D.; Varetto, G.; Bucci, E.; Maniero, F.; Guiot, C. Fractal parameters and vascular networks: facts & artifacts. *Theor. Biol. Med. Modell.* **2008**, *5*, No. 12.

(17) Mansoory, M. S.; Oghabian, M. A.; Homayoun, A.; Shahbabaie, A. Analysis of resting-state fMRI topological graph theory in methamphetamine drug users applying box-counting fractal dimension. *Basic Clin. Neurosci.* **2017**, *8*, 371−386.

(18) Li, J.; Du, Q.; Sun, X. An improved box-counting method for image fractal dimension estimation. *Pattern Recognit.* **2009**, *42*, 2460−2469.

(19) Bouda, M.; Caplan, J. S.; Saiers, J. E. Box-counting dimension revisited: Presenting an efficient method of minimizing quantization error and an assessment of the self-similarity of structural root systems. *Front. Plant Sci.* **2016**, *7*, No. 149.

(20) Blenkinsop, T. G. In *Applications of fractal geometry to mineral exploration*, SEG Predictive Mineral Discovery Under Cover: Extended Abstracts, 2004; pp 158−161.

(21) Soumya, S.; Swapna, M. S.; Raj, V.; Pillai, M.; Sankararaman, S. Fractal as a potential tool for surface morphology of thin films. *Eur. Phys. J. Plus* **2017**, *132*, No. 551.

(22) Mandelbrot, B. B. *The Fractal Geometry of Nature*; Henry Holt & Company Co Pte Ltd: New York, 2010.

(23) Xia, Y.; Cai, J.; Wei, W.; Hu, X.; Wang, X.; Ge, X. A new method for calculating fractal dimensions of porous media based on pore size distribution. *Fractals* **2018**, *26*, No. 1850006.

(24) Nair, G. G.; Nair, A. S. Fractality of numeric and symbolic sequences. *IEEE Potentials* **2010**, *29*, 36−39.

(25) Liu, Y.; Chen, L.; Wang, H.; Jiang, L.; Zhang, Y.; Zhao, J.; Wang, D.; Zhao, Y.; Song, Y. An improved differential box-counting method to estimate fractal dimension of gray-level images. *J. Vis. Commun. Image R.* **2014**, *25*, 1102−1111.

(26) Elejalde-Cadena, N. R.; Cabrera-Hernández, J. S.; Hernández-Rivera, R.; Moreno, A. Searching for a Clue to Characterize a Crystalline Dinosaur's Eggshell of Baja California, Mexico. *ACS Omega* **2020**, *5*, 25936−25946.

(27) Mikhailov, K. E. Special Papers in Palaeontology. In *Fossil and Recent Eggshell in Amniotic Vertebrates: Fine Structure, Comparative Morphology and Classification*, Mikhailov, A., Ed.; CRC Press: Wiley, London, 1997; p 80.

(28) Mikhailov, K. E.; Bray, E. S.; Hirsch, K. F. Paratoxonomy of fossil eggs remains (Veterovata): Principles and application. *J. Vertebr. Paleontol.* **1996**, *16*, 763−769.

(29) Carpenter, K. *Eggs, Nets, and Baby Dinosaurs. A Look at Dinosaur Reproduction*,Farlow, J. O., Ed.; CRC Press: Indiana University: Indiana, 1999; p 141.

(30) Tarhan, L. G.; Hood, A. V. S.; Droser, M. L.; Gehling, J. G.; Briggs, D. E. G.; Gaines, R. R.; Robbins, L. J.; Planavsky, N. J. Petrological evidence supports the death mask model for the preservation of Ediacaran soft-bodied organism in South Australia. *Geology* **2019**, *47*, No. e473.

(31) Suarez, C. A.; Kohn, M. J. Effect of climate change on humic substances and associated impacts on the quality of surface water and groundwater: review. *Geochim. Cosmochim. Acta* **2020**, *268*, 277−295.

(32) Kim, C. B.; Al-Aasm, I. S.; Ghazban, F.; Chang, H. W. Stable Isotopic composition of dinosaur eggshells and pedogenic carbonates in the upper cretaceous seonso formation, South Korea: Paleoenvironmental and diagenetic implications. *Cretaceous Res.* **2009**, *30*, 93−99.

(33) Sharp, Z. *Principles of Stable Isotope Geochemistry*; Pearson Prentice Hall Co Pte Ltd: Michigan, 2007.

https://dx.doi.org/10.1021/acsomega.1c00478
ACS Omega 2021, 6, 7887−7895